Complementarity and redundancy of IL-22-producing innate lymphoid cells

Lucille C. Rankin, Mathilde J. H. Girard-Madoux, Cyril Seillet, Lisa A. Mielke, Yann Kerdiles, Aurore Fenis, Elisabeth Wieduwild, Tracy Putoczki, Stanislas Mondot, Olivier Lantz, et al.

Complementarity and redundancy of IL-22-producing innate lymphoid cells

Lucille C. Rankin[1,13,14], **Mathilde J. H. Girard-Madoux**[2,14], **Cyril Seillet**[1,15], **Lisa A. Mielke**[1,15], **Yann Kerdiles**[2,15], **Aurore Fenis**[2], **Elisabeth Wieduwild**[2], **Tracy Putoczki**[1], **Stanislas Mondot**[3], **Olivier Lantz**[4], **Dieter Demon**[5], **Anthony T. Papenfuss**[1], **Gordon K. Smyth**[1,6], **Mohamed Lamkanfi**[5], **Sebastian Carotta**[1,7], **Jean-Christophe Renauld**[8], **Wei Shi**[1,9], **Sabrina Carpentier**[10], **Tim Soos**[11], **Christopher Arendt**[11], **Sophie Ugolini**[2], **Nicholas D. Huntington**[1], **Gabrielle T. Belz**[1,16], and **Eric Vivier**[2,12,16]

[1]The Walter and Eliza Hall Institute of Medical Research, and Department of Medical Biology, University of Melbourne, Victoria 3052 Australia; and Department of Medical Biology, University of Melbourne, Parkville 3010, Australia

[2]Centre d'Immunologie de Marseille-Luminy, Université d'Aix-Marseille UM2, Inserm, U1104, CNRS UMR7280, 13288 Marseille, France

[3]Labex Milieu Intérieur, Institut Pasteur, 75724 Paris, France

[4]Laboratoire d'Immunologie and Inserm U932, Institut Curie, 75005 Paris, France

[5]Inflammation Research Center, VIB; and Department of Biochemistry, Ghent University, 9052 Ghent, Belgium

[6]Department of Mathematics and Statistics, University of Melbourne, Parkville 3010, Australia

[7]Boehringer-Ingelheim RCV, Dr-Boehringer-Gasse 5-11, 1120 Vienna, Austria

[8]Ludwig Institute for Cancer Research Ltd and Experimental Medicine Unit, Catholic University of Louvain, Brussels, Belgium

[9]Department of Computing and Information Systems, University of Melbourne, Parkville 3010, Australia

[10]MI-mAbs consortium Aix-Marseille University, CIML, 13288 Marseille, France

---

Correspondence to: belz@wehi.edu.au and vivier@ciml.univ-mrs.fr.
[13]Present address: Weill Cornell Medical College, Cornell University, New York, New York 10021, USA
[14]These authors contributed equally to this work
[15]These authors contributed equally to this work
[16]These authors contributed equally to this work

AUTHOR CONTRIBUTIONS

L.R., M.G.M., C.S., L.A.M. and Y.K. designed the research, performed experiments and analyzed the data; A.F., E.W., S.M., L.M., J.G., T.P., T.P. performed experiments and analyzed the data; W.S and G.K.S performed bioinformatic analyses of RNAseq data. O.L., D.D., M.L., J.C.R., C.A., S.U., S.C. and N.D.H. provided key reagents; G.B. and E.V. designed the research, supervised the study, and wrote the manuscript with the help of the other co-authors.

Accession codes. GEO: mRNA-seq, GSE72909.

COMPETING FINANCIAL INTERESTS

E.V. is the cofounder and a shareholder of Innate Pharma. The other authors have no conflicting financial interest to declare.

[11]Bioinnovation, SANOFI, Boston, USA

[12]Immunologie, Hôpital de la Conception, Assistance Publique – Hôpitaux de Marseille, 13385 Marseille, France

Abstract

Intestinal T cells and group 3 innate lymphoid cells (ILC3) control the composition of the microbiota and gut immune responses. Within the gut there coexists ILC3 subsets which either express or lack the Natural cytoxicity receptor (NCR) NKp46. We identify here the transcriptional signature associated with the T-bet-dependent differentiation of NCR^- ILC3 into NCR^+ ILC3. Contrary to the prevailing view, we show by conditional deletion of the key ILC3 genes *Stat3*, *Il22*, *Tbx21* and *Mcl1* that NCR^+ ILC3 were redundant for the control of mouse colonic infections with *Citrobacter rodentium* in the presence of T cells. However, NCR^+ ILC3 were essential for cecum homeostasis. Our data show that interplay between intestinal ILC3 and adaptive lymphocytes results in robust complementary fail-safe mechanisms ensuring gut homeostasis.

Dysregulation of intestinal barrier function disrupts gut microbiota and results in inflammation, diarrhea and chronic disease. Mucosal immunity is essential to control the composition of gut commensal flora and maintain health in the face of continual exposure to potentially pathogenic bacteria in the gastrointestinal tract. Interleukin 22 (IL-22) plays a crucial role in this immune control of gut commensal and pathogenic bacteria and is secreted by a heterogeneous population of lymphocytes expressing the nuclear hormone receptor RORγt (encoded by the gene *Rorc*)[1], including subsets of T helper cells (T_H17, T_H22) and group 3 innate lymphoid cells (ILCs) [2-7].

ILC3 are a heterogeneous population of innate lymphoid cells particularly abundant at mucosal sites. They can be divided into three main subsets, based on their role during embryogenesis and cell surface expression of the NCR, NKp46 (hereafter referred to as NCR^+ or NCR^- cells). NCR^- ILC3 comprise lymphoid-tissue inducer (LTi) cells, which were originally found in the fetus and are required for the development of lymph nodes and Peyer's patches [8]. LTi cells do not require expression of the transcription factor PLZF[9], and can be divided into $CD4^-$ and $CD4^+$ cells. Another subset of NCR^- ILC3 requires PLZF, and give rise to NCR^+ ILC3 in a T-bet- and Notch-dependent manner [10, 11]. NCR^- ILC3 can promote colitis in a model of inflammatory bowel disease [12]. By contrast, NCR^+ ILC3 have been shown to be essential for regulating the balance between commensal and pathogenic bacteria through their IL-23-driven production of IL-22, particularly during *Citrobacter rodentium* infection [13, 14]. *C. rodentium* is a Gram negative mouse-restricted pathogenic bacterium that can be used as a model of the human enteric pathogens enteropathogenic *Escherichia coli* (EPEC) and enterohemorrhagic *E. coli* (EHEC). It colonizes the intestinal mucosa, leading to the formation of attaching and effacing lesions that result from the effacement of the brush border microvilli. IL-22 is essential for the control of *C. rodentium* infection, as it stimulates the secretion of antimicrobial peptides and protects epithelial function [15]. As a consequence, animals lacking this cytokine rapidly succumb to the disease [16]. NCR^+ ILC3 play a critical role in protection against *C. rodentium* in mice globally deficient for genes also expressed in B or T cells, such as *Rag2, Tbx21* or *Cxcr6*

[11, 13, 14, 17]. However, these mouse models have profound or partial immunodeficiencies, confounding the interpretation of the findings and the selective contributions of NCR^- and NCR^+ ILC3. Overall, the analysis of ILC3 biology has been hampered by the lack of models selectively targeting these cells. Here, we explored the biology of innate producers of IL-22 in mouse conditional deletion models targeting NCR^+ ILC3 but preserving B and T cells, to elucidate the specific contributions of NCR^+ ILC3 to intestinal protection. Our comprehensive analysis of gut ILC3 revealed the redundant role of NCR^+ ILC3 in the control of *C. rodentium* infection in immunocompetent hosts, and a selective role of NCR^+ ILC3 in cecum homeostasis.

Results

Expression profiles of ILC3 subsets

To date, $ROR\gamma t^+$ IL-22-producing ILC3s have been divided into at least four different subsets, including T-bet-independent NCR^- ILC3 comprising $CD4^+NKp46^-$ and $CD4^-NKp46^-$ ILC3, and T-bet-dependent NCR^+ ILC3 comprising $NCR^+ROR\gamma t^{int}$ and $NCR^+ROR\gamma t^{hi}$ ILC3 [18, 19]. We investigated the relationships between these four ILC3 populations, by isolating $CD4^+NCR^-$ ($CD4^+$), $CD4^-NCR^-$ (DN), $NCR^+ROR\gamma t^{int}$ and $NCR^+ROR\gamma t^{hi}$ ILC3 from the small intestine of $Rorc^{+/GFP}$ reporter mice (Fig. 1a) and performing a genome-wide transcriptome analysis by RNA sequencing (RNAseq). Within the NCR^- ILC3 subsets, the transcriptional profiles of the $CD4^+NCR^-$ and $CD4^-NCR^-$ ILC3 were almost identical (Table 1), indicating that they could be considered as a single population of NCR^- ILC3. Similarly, $NCR^+ROR\gamma t^{int}$ and $NCR^+ROR\gamma t^{hi}$ NCR^+ILC3 had very similar transcriptional programs (Table 1), differing only for the expression of a set of receptors guiding localization and including *Ccl5, Cxcr5 Ccl4* and *Ccr5* (Supplementary Table 1). Thus, $NKp46^+ROR\gamma t^{int}$ and $NKp46^+ROR\gamma t^{hi}$ cells were also extremely similar and could be considered as a single population of NCR^+ ILC3. By contrast, robust differences in transcriptional profile were found between NCR^- ILC3 and NCR^+ ILC3. The expression of genes encoding transcription factors, such as *Idb2, Gata3* and *Rorc,* was similar in the different subsets, whereas the expression of *Tbx21* and *Prdm1* was upregulated in NCR^+ ILC3. Genes encoding a number of other transcriptional regulators were also found to be differentially expressed, including interferon regulatory factor 8 (*Irf8*), which was upregulated, and *Batf3* and *Tox2,* which were downregulated in NCR^+ ILC3. Thus, NCR^+ ILC3 and NCR^- ILC3 are distinct ILC3 subsets with different gene transcription programs consistent with microarray analysis [20], validating our RNAseq approach.

The impact of T-bet on ILC3

T-bet is key to the differentiation of NCR^- ILC3, as NCR^+ ILC3 are absent from *Tbx21*-deficient mice [10, 11, 21], but the mechanisms by which T-bet affects ILC3 maturation are unclear. We investigated the transcriptional program of ILC3 isolated from $Rorc^{gfp/+}Tbx21^{+/-}$ mice, which lack one copy of T-bet. Given that $Rorc^{gfp/+}Tbx21^{+/-}$ mice have a heterogeneous phenotype, we reasoned that the loss of one allele would uncover differential regulation by T-bet without the complete loss of NCR^+ ILC3, which remain present albeit at a lower frequency (Fig. 1a). We then performed two types of analysis on the RNAseq transcriptional profile dataset obtained from the following eight ILC3 populations:

$CD4^+NCR^-$, $CD4^-NCR^-$ (DN), $NCR^+ROR\gamma t^{int}$ and $NCR^+ROR\gamma t^{hi}$ from *Tbx21*$^{+/+}$ and $CD4^+NCR^-$, $CD4^-NCR^-$ (DN), $NCR^+ROR\gamma t^{int}$ and $NCR^+ROR\gamma t^{hi}$ from *Tbx21*$^{+/-}$ mice. We first compared the list of genes differentially expressed between NCR^- ILC3 ($CD4^+$and $CD4^-$) and NCR^+ ILC3 ($ROR\gamma t^{int}$ and $ROR\gamma t^{hi}$) in control mice with that for *Tbx21*$^{+/-}$ mice. In total, 674 genes displayed differences in expression by a factor of at least two between NCR^- ILC3 and NCR^+ ILC3 in wild-type mice; 324 of these genes did not display differential expression between these two cell types in *Tbx21*$^{+/-}$ mice (**data not shown**). Thus, during the transition between NCR^- and NCR^+ ILC3, about 50% of genes were affected by the loss of a single copy of T-bet, indicating that T-bet guides a substantial component of the NCR^+ ILC3 developmental program. Second, the gene expression profiles of ILC3 from *Tbx21*$^{+/-}$ mice were compared with those from the corresponding wild-type ILC3 populations. We found no role for T-bet in $CD4^+$ and $CD4^-$ $NKp46^-$ ILC3. Therefore, as expected, in NCR^- ILC3 populations ($CD4^+$ and $CD4^-$), very few genes were differentially expressed between *Tbx21*$^{+/+}$ and *Tbx21*$^{+/-}$ cells. However, significant differences in transcriptional profile were observed between *Tbx21*$^{+/+}$ and *Tbx21*$^{+/-}$ NCR^+ ILC3 ($ROR\gamma t^{int}$ and $ROR\gamma t^{hi}$): analyses of at least two-fold differences in expression between *Tbx21*$^{+/+}$ and *Tbx21*$^{+/-}$ NCR^+ ILC3 showed that 72 genes were upregulated and 86 downregulated in the wild-type cells (Supplementary Table 2). This enabled us to investigate the gene programs specifically regulated by T-bet during generation of the NCR^+ ILC3 subset (Fig. 1b). Interestingly, 70% of the genes found to be down-regulated on NCR^+ ILC3 in the absence of T-bet were highly expressed on NCR^+ ILC3 compared to NCR^- ILC3. Loss of a single allele of T-bet affected communication between innate and adaptive cells through cytokine or chemokine regulation *via Il2r* and interferon signaling through the Jak-Stat pathway*, Il22, Ccl4* and *Ccl5*. T-bet also regulated a number of important gene clusters known to be preferentially associated with effector functions such as cytotoxicity and expressed by NK cells (e.g. *Gzme, Gzma, Ifnγ* and *Il12rb*). These gene clusters also included members of the killer-cell lectin-like receptor family: *Klri1* (Ly49E1), *Klrd1* (CD94), *Klrb1c* (CD161, NK1.1) and *Klrc2* (NKG2C). Consistent with the genomic analyses, the T-bet-dependent regulation of NK1.1 and CD94-NKG2 heterodimers on NCR^+ ILC3 was confirmed at the protein level (Fig. 1c). Thus, in addition to being required for the development of NCR^+ ILC3 from NCR^- ILC3, T-bet appears to play an important role in the recognition, effector function and migration of NCR^+ ILC3 within tissues. T-bet is also the major driver of the 'NK-ness' program of NCR^+ ILC3.

NCR^+ ILC3 are dispensable in immunocompetent mice

The pathway analysis of ILC3 transcriptomic data revealed that the set of genes expressed in NCR^+ ILC3 and downregulated in *Tbx21*$^{+/-}$ mice was enriched in genes involved in the control of gastrointestinal diseases and bacterial infections (Fig. 1b). Consistent with these data, NCR^+ ILC3 were reported pivotal in protection against *C. rodentium* in various models of immunodeficient mice [11, 13, 14, 17]. We then investigated the role of the IL-22 produced by NCR^+ ILC3 during the course of *C. rodentium* infection. We used a previously undescribed model of *Il22*$^{eGFP/eGFP}$*Ncr1*-iCre mice (Supplementary Fig. 1), in which NCR^+ ILC3 were unable to produce IL-22 (Fig. 2a). We also crossed *Ncr1*-iCre mice with *Stat3*$^{fl/fl}$ mice, for the selective abolition of STAT3-dependent signals in NCR^+ ILC3, as the transcription factor STAT3 is required for the production of IL-22 by ILC3 and Th17 cells, and the ablation of

Stat3 in RORγt$^+$ lymphocytes leads to increased morbidity and mortality after *C. rodentium* infection [22]. NCR$^+$ ILC3 were unable to produce IL-22 in both *Il22*$^{eGFP/eGFP}$*Ncr1*-iCre and *Stat3*$^{fl/fl}$*Ncr1*-iCre mice (Fig. 2a) but both types of mice were resistant to *C. rodentium* infection, as no deaths, weight loss, histological abnormalities in the gut or increase in bacterial dissemination relative to controls were observed (Fig. 2b and Fig. 3). This resistance could not be accounted for by a compensatory increase in IL-22 production by NCR$^-$ ILC3, which were present in normal numbers and produced normal amounts of the cytokine (Supplementary Fig. 1c,d and Supplementary Fig. 2). By contrast, treatment with blocking anti-IL-22 led to severe colitis and the premature death of wild-type mice challenged with the same dose of *C. rodentium* (Fig. 2b), as previously described [16]. Thus, IL-22 was essential for resistance to *C. rodentium* but the production of IL-22 by NCR$^+$ ILC3 was dispensable.

We then ablated NCR$^+$ ILC3 to address their contribution to the control of *C. rodentium* infections more generally. We directly abolished *Tbx21* expression in NCR$^+$ ILC3, by crossing *Ncr1*$^{iCre/+}$ mice with *Tbx21*$^{fl/fl}$ mice. Consistent with previous findings, the numbers of NKp46$^+$ RORγt$^-$ cells and NCR$^+$ ILC3 were much smaller in the small intestine and colon of *Tbx21*$^{fl/fl}$*Ncr1*-iCre mice than in controls (Fig. 4 and Supplementary Fig. 3a). However, *Tbx21*$^{fl/fl}$*Ncr1*-iCre mice were resistant to *C. rodentium* infection, as no deaths, weight loss, histological abnormalities in the gut or increase in bacterial dissemination relative to controls were observed in *Tbx21*$^{fl/fl}$*Ncr1*-iCre mice (Fig. 2b and Supplementary Fig. 3b-d). A marked increase in the number of IL-22-producing NCR$^-$ ILC3 was observed in the *Tbx21*$^{fl/fl}$*Ncr1*-iCre mice (Fig. 4 and Supplementary Fig. 3a), potentially compensating for the loss of NCR$^+$ ILC3 in this model. We thus addressed the role of ILC3 during *C. rodentium* infection further, by generating another model of NCR$^+$ ILC3 deficiency by crossing *Ncr1*$^{iCre/+}$ mice with *R26*$^{DTA/+}$ (*Rosa*-DTA) mice. A near-complete absence of NCR$^+$ ILCs (both NCR$^+$ RORγt$^-$ and NCR$^+$ ILC3), with no increase in NCR$^-$ ILC3 numbers, was observed in the small intestine and colon of *R26*$^{DTA/+}$*Ncr1*-iCre mice (Fig. 4 and Supplementary Fig. 4a, b). When *R26*$^{lsl\text{-}DTA/+}$*Ncr1*$^{iCre/+}$ mice were infected with *C. rodentium*, no morbidity or mortality was recorded (Fig. 2b). These findings are supported by the lack of difference between *R26*$^{DTA/+}$*Ncr1*-iCre mice and controls in terms of colon length and histology, and bacterial dissemination, as assessed by the number of cfu in the feces, spleen and liver (Fig. 5). We further monitored the immune response to *C. rodentium* infection in these mice and we found no statistically significant differences in other parameters, such as the cellularity of the gut lamina propria for CD4$^+$ T cells, CD8$^+$ T cells, B cells, Ly6G$^+$Ly6C$^+$ myeloid cells and MHC class II$^+$ CD11c$^+$ dendritic cells, or the ability of mesenteric lymph node and splenic CD4$^+$ T cells and CD8$^+$ T cells to produce IL-17A or IFN-γ upon *in vitro* re-stimulation (Supplementary Fig. 4c-e). Cytokine (IFN-γ, IL-17A, Il-1β, IL-6, KC, TNF-α and IL-10) determinations in gut extracts revealed no differences between *R26*$^{DTA/+}$*Ncr1*-iCre mice and controls (Supplementary Fig. 4f).

Mcl-1 is an anti-apoptotic protein induced by common γ chain (γc) receptor signaling and required for the maintenance of NK cells *in vivo* [23]. We investigated whether Mcl-1 was also required for the maintenance of NCR$^+$ ILC3 in the gut. Both NCR$^+$ RORγt$^-$ and NCR$^+$ ILC3 populations were absent from *Mcl1*$^{fl/fl}$*Ncr1*-iCre mice (Fig. 4). These data demonstrate the key role of Mcl-1 in maintaining all NKp46$^+$ ILC *in vivo*. *Mcl1*$^{fl/fl}$*Ncr1*-

iCre mice constitute another model of immune deficiency in which NCR$^+$ ILC3 are absent but NCR$^-$ ILC3 and T cells are unaffected. We challenged *Mcl1*$^{fl/fl}$*Ncr1*-iCre mice with *C. rodentium*. As for *R26*$^{DTA/+}$*Ncr1*-iCre mice, *Mcl1*$^{fl/fl}$*Ncr1*-iCre mice were resistant to the infection (Fig. 2b), with no signs of disease or bacterial dissemination detected by histology, or on the basis of colon length or the number of cfu in the spleen and liver (Supplementary Fig. 5). Thus, the results for five different genetic models converged to reveal that NCR$^+$ ILC3 were dispensable for the control of *C. rodentium* infection in immunocompetent mice.

The lower amounts of IL-22 production by ILC3 in *Ahr*-deficient mice has been shown to allow the proliferation of commensal segmented filamentous bacteria (SFB), which are known to promote the development of Th17 cells [24]. We therefore also investigated the consequences of a lack of NCR$^+$ ILC3 for the gut microbiota at steady state, by deep sequencing. No difference in the presence of particular bacterial families or SFB numbers in the feces, or in Th17 counts in the small intestine was detected in comparisons of *R26*$^{DTA/+}$*Ncr1*-iCre mice and control mice housed in the same conditions (Supplementary Fig. 6a-c). Similarly, the bacterial families present in the gut of *Mcl1*$^{fl/fl}$*Ncr1*-iCre mice did not differ significantly from those present in the gut of controls (not shown). Thus NCR$^+$ ILC3 deficiency had no impact on the gut microbiota in immunocompetent hosts at steady state.

A role for NCR$^+$ ILC3 in immunodeficient mice

The results presented above contrast with previous reports of a critical role for NCR$^+$ ILC3 in protection against *C. rodentium in Rag2-, Tbx21-, Cxcr6-* or *Id2*-deficient mice [11, 13, 14, 17, 25]. As all these mouse models display profound or partial immunodeficiencies, we investigated the role of NCR$^+$ ILC3 in immunodeficient and immunocompetent mice directly, by crossing *R26*$^{DTA/+}$*Ncr1*-iCre mice with *Rag2*$^{-/-}$ mice, which lack T and B cells. *Rag2*$^{-/-}$*Ncr1*$^{iCre/+}$ mice, *Rag2*$^{-/-}$*R26*$^{DTA/+}$*Ncr1*-iCre and *R26*$^{DTA/+}$*Ncr1*-iCre littermates were then infected with *C. rodentium* and their resistance to bacterial infection was evaluated by monitoring mouse weight and survival. Consistent with our previous findings, *R26*$^{DTA/+}$*Ncr1*-iCre mice were resistant to *C. rodentium* (Fig. 6a and Fig. 6b). After initial control of the infection, *Rag2*$^{-/-}$*Ncr1*$^{iCre/+}$ mice lost weight and started to succumb to the disease on day 17 post-infection (Fig. 6a and Fig. 6b), as previously reported [26]. *Rag2*$^{-/-}$*R26*$^{DTA/+}$*Ncr1*-iCre mice were even more susceptible to the infection than their *Rag2*$^{-/-}$*Ncr1*-iCre littermates, as shown by their greater weight loss on days 12 to 14 post-infection, with the first mice dying on day 13 and all mice dead by day 22, as opposed to day 26 for the *Rag2*$^{-/-}$*Ncr1*-iCre mice (Fig. 6a and Fig. 6b). Thus, NCR$^+$ ILC3 cells were not essential for the control of *C. rodentium* in immunocompetent hosts, whereas they contributed to the control of *C. rodentium* in immunodeficient mice.

Role of NCR$^+$ ILC3 in cecum homeostasis

In contrast to the lack of impact of NCR$^+$ ILC3-deficiency in the small intestine or the bulk of the colon, the absence of NCR$^+$ ILC3 in *Mcl1*$^{fl/fl}$*Ncr1*-iCre mice during *C. rodentium* infection resulted in a decrease in cecum size, together with ulceration and bleeding (Fig. 7a). These pathological features in the cecum were also observed when *Stat3*$^{fl/fl}$*Ncr1*-iCre mice were infected with *C. rodentium* (Fig. 7b). They were accompanied by crypt

hyperplasia and inflammation, as shown by the H&E staining of cecum sections (Fig. 7c). At steady state, no alteration to the cecum, small intestine or colon was observed in any of the five genetic models of NCR$^+$ ILC3 deficiency (*Mcl1*$^{fl/fl}$*Ncr1*-iCre, *R26*$^{DTA/+}$*Ncr1*-iCre, *Tbx21*$^{fl/fl}$*Ncr1*$^{iCre/+}$, *Il22*$^{eGFP/eGFP}$*Ncr1*-iCre and *Stat3*$^{fl/fl}$*Ncr1*$^{iCre/+}$) (data not shown). Thus, NCR$^+$ ILC3 play a critical role in protecting the cecum during *C. rodentium* infection, and this function is abolished in conditions in which NCR$^+$ ILC3 cannot produce IL-22.

We further dissected the critical role of NKp46$^+$ cells in the control of cecum homeostasis during *C. rodentium* infection, by examining the regional distribution of gut ILCs. *C. rodentium* is a colonic infection, but it begins in the cecum. In wild-type mice the protective role of NKp46$^+$ cells was associated with a high frequency of NCR$^+$ ILC3 in the cecum at steady state, contrasting with the low frequency of NCR$^+$ ILC3 in the colon (Fig. 7d). At the junction of the small intestine and the colon, the cecum was globally characterized by a distribution of ILCs with features of both the small intestine, with a high frequency of NCR$^+$ ILC3, and the colon, with a low frequency of NCR$^-$ ILC3 (Fig. 7d). In wild-type mice this distribution of intestinal ILCs was profoundly altered over the course of *C. rodentium* infection, as the frequency of NCR$^+$ ILC3 was considerably lower in the cecum and colon (Fig. 7e). The causes and consequences of these changes remain to be fully explored. A characteristic feature of cecal NCR$^+$ ILC3 is their high density of NK1.1 cell surface expression, contrasting with the low density of NK1.1 at the surface of small intestine NCR$^+$ ILC3 and the intermediate expression on colon NCR$^+$ ILC3 (Supplementary Fig. 7a). The role of NK1.1 is unknown, but these data provide an explanation for the deleterious effect of anti-NK1.1 treatment on *Rag2*$^{-/-}$ mice infected with *C. rodentium* reported in a previous study [14]. Indeed, treatment with depleting anti-NK1.1 antibodies decreased the numbers of NCR$^+$ ILC3, particularly in the cecum, but also in the colon to some extent, whereas it had no effect on NCR$^+$ ILC3 numbers in the small intestine (Supplementary Fig. 7b). Anti-NK1.1 antibodies also depleted NKp46$^+$RORγt$^-$ cells, including NK cells, ILC1 and ex-ILC3 (Supplementary Fig. 7b). However, all NKp46$^+$RORγt$^-$ cells produce interferon-γ (IFN-γ) and IFN-γ-deficient mice are not more sensitive to *C. rodentium* infection [26], by contrast to IL-22-deficient mice [16]. Overall, these results suggest that cecal NK1.1$^+$ NCR$^+$ ILC3 are involved in the control of *C. rodentium* infection, through their production of IL-22.

Discussion

The aim of this study was to dissect the biology of NCR$^+$ ILC3, a subset of IL-22-producing innate lymphoid cells of the gut, and their interplay with adaptive immunity in the context of a colonic infection, in the *C. rodentium* model.

By using *Ncr1*$^{iCre/+}$ mice, in which NCR$^+$ cells are selectively targeted, we were able to highlight the intrinsic role of *Tbx21, Mcl1* and *Stat3* in the development, maintenance and function of NCR$^+$ ILC3. The generation of *Il22*$^{eGFP/eGFP}$*Ncr1*-iCre mice made it also possible to carry out functional fate mapping of IL-22-producing NCR$^+$ ILC3, without detectable cofounding effects due to under-reporting for the *Il22*-Cre allele [27]. Using these mice, we detected no IL-22 production by intestinal RORγt$^-$NKp46$^+$ cells, including NK cells, ILC1 and 'ex-ILC3' [28]. These findings contrast with those of other studies reporting

the production of IL-22 by human and mouse NK cells from various inflamed tissues [29, 30, 31, 32, 33], and they lead us to reconsider whether RORγt$^-$ ILCs could produce IL-22.

We also show that neither the production of IL-22 by NCR$^+$ ILC3, nor the cells themselves were essential for the control of intestinal infection by *C. rodentium* in immunocompetent hosts. In these mice, NCR$^+$ ILC3 did not control the gut commensal microbiota either. Previous studies have shown that NCR$^+$ ILC3 play a critical role in protection against *C. rodentium* in mice with profound or partial immunodeficiencies [11, 13, 14, 17]. Our results are consistent with previous reports [10, 34], and challenge the current dogma in revealing that NCR$^+$ ILC3 are not essential for the control of intestinal infections in the presence of T cells. We also show that NCR$^+$ ILC3 can confer some protection against *C. rodentium* if T cells are absent. The critical role of IL-22-producing T cells in the control of *C. rodentium* infection has already been demonstrated [26]. Previous studies investigated the contributions of T_H17 and T_H22 cells during the late phases of *C. rodentium* infection [26], and suggested that the IL-22 produced by the total ILC3 population (consisting of multiple subsets) was important early in *C. rodentium* infection, but that once T cells were activated, ILC3 appeared to be dispensable [13, 16, 22, 26, 27, 35]. Thus, NCR$^+$ ILC3, NCR$^-$ ILC3 and T_H17 or T_H22 cells can display some functional redundancy. It has also been suggested that NCR$^-$ ILC3 provide an adequate barrier to *C. rodentium* infection [36], as they produce large amounts of IL-22 in the gut [27]. However, we show here that these cells are not sufficient to confer protection against *C. rodentium* in T cell-compromised mice in the presence or absence of NCR$^+$ ILC3. Nevertheless, formal elucidation of the role of NCR$^-$ ILC3 in the control of the gut commensal and pathogenic microbiota awaits the development of tools for the selective ablation of this cell population.

The interplay between T cells and ILCs is a matter of great interest. ILCs can interact with CD4 T cells via MHC class II molecules, limiting pathological adaptive immune cell responses to commensal bacteria [37]. It has also been suggested that T cells function as antigen-specific sensors for the activation of ILCs, to amplify and instruct local immune responses [38]. We describe here another type of relationship between T cells and ILC3, in which NCR$^+$ ILC3 can partly overcome the lack of T cells for protection against the pathogenic bacterium *C. rodentium*, but become redundant if T cells are present. This is, to our knowledge, the first formal demonstration of redundancy between T cells and ILCs. T cells and ILCs have evolved similar effector functions despite their use of different recognition strategies: a germline-encoded receptor for ILCs vs. antigen receptors generated by site-specific somatic recombination for T cells. It is thus tempting to speculate that ILC3 and T_H17 and T_H22 cells have co-evolved, leading to the selection of robust fail-safe mechanisms for ensuring adequate control of the commensal gut microbiota and protection against intestinal infections. Selective pressure for redundancy might have led to the similarities between ILCs and T cells in terms of their distribution and effector function.

Unexpectedly, severe pathological features were observed in the cecum when NCR$^+$ ILC3 were ablated. Similar severe cecal lesions were also observed in IL-22-deficient mice upon infection with *C. rodentium* [16], supporting a role for NCR$^+$ ILC3, the only NKp46$^+$ cells that can produce IL-22, in the cecal phenotype. The cecum is the first site in the

gastrointestinal tract to be colonized by *C. rodentium* during infection, with invasion of the colon occurring later (~day 8) [39]. We thus propose a model in which NCR^+ ILC3 are redundant with T cells for protection against lethality and colon disease during intestinal infections, but critical for protecting against cecum damage at the earliest stage of infection. The cecum is a blind pouch at the junction between the small intestine and the large intestine. It is a source of bacteria and it is also linked to the appendix in humans and mice, in which it is referred to as the cecal patch. The appendix has generally been seen as an evolutionary vestige, but recent phylogenetic studies challenge the apparent lack of function of the cecum and appendix [40]. In particular, it has been suggested that the cecum and appendix provide an important reservoir for maintenance of the gut flora, which is anatomically protected from the intestinal lumen and could allow seeding of the gut after dysbiosis. Our data demonstrating that NCR^+ ILC3 play a critical role in the homeostasis of the cecum upon bacterial infection opens up new possibilities for delineating the role of ILC3 in the pathophysiology of the cecum and appendix and in maintaining the health of the intestinal tract. In particular, it will be interesting to determine whether the balance between NCR^- ILC3 and NCR^+ ILC3 is involved in the still unknown mechanisms leading to appendicitis and resistance or susceptibility to inflammatory bowel diseases, as these two conditions may be related [41].

Online Methods

Mice

All the mice used were bred and maintained in specific pathogen-free facilities at the WEHI or CIML. C57BL/6, *Rag2*$^{tm1.1Flv}$ × *Il2rg*$^{tm1.1Flv}$ (Rag2γc), *Stat3*$^{fl/fl}$ [42], *Rorc*^{GFP} [43], *Tbx21*$^{-/-}$ [44], *Mcl1*$^{fl/fl}$ [23], *Ncr1*-iCre [45], *R26*$^{DTA/+}$ (Rosa-DTA) and *Rag2*$^{-/-}$ × *R26*$^{DTA/+}$ mice were used. All animal experiments were performed with the approval of either the Animal Ethics Committees of the Walter and Eliza Hall Institute according to National Health and Medical Research Council (NHMRC) of Australia guidelines, or the Animal Ethics Committees of the Ciml and in accordance with European laws.

Generation of *Il22*$^{fl/fl}$ mice

A loxP site was inserted downstream from *Il22* exon 1 and a reporter/selection cassette (loxP-SA-P2A-DTR-T2A-eGFP-polyA-frt-Hyg-frt) was inserted downstream from the *Il22* polyA sequence (Supplementary Fig. 1a). The genomic coordinates for the floxed region are: NCBIM37: chr10:117,642,470-117,647,823. *Il22*$^{eGFP/eGFP}$*Ncr1*-iCre mice were obtained at Mendelian frequencies; they developed normally and were fertile.

Inoculation with *Citrobacter rodentium*

Overnight cultures of bacterial strains were centrifuged and the pellet was resuspended in PBS. Food was withdrawn for 8 hours before infection, and the six- to nine-week-old mice (male and female) were inoculated by oral gavage with 200 µl of a suspension of 2×10^9 or 1×10^{10} cfu of *C. rodentium*. The viable count of the inoculum was determined retrospectively by plating dilutions of the inoculum on plates with appropriate antibiotics, or on McConkey agar (CM0007B; Oxoid) plates supplemented with 0.68% sodium thiosulfate (Sigma) and 0.08% ammonium citrate (Sigma). Animals were allocated to experimental

groups so as to ensure even distributions of age, sex and weight. Infection experiments were carried out at least twice, regardless of sample size, to ensure reproducibility, and results shown correspond to combined experimental data from all repeats. Mice were weighed daily and feces were collected at two- to four-day intervals for bacterial counts. The viable bacterial count per 100 mg of feces was determined by plating serial dilutions feces, in duplicate, on medium containing selective antibiotics. The colon and small intestine were then harvested and their length was measured. For the assessment of bacterial dissemination, the spleen and liver were collected from infected mice, weighed and homogenized. The homogenates were then cultured overnight at 37°C on LB agar plates containing 10 mM naladixic acid or McConkey agar plates, as described above.

Isolation of lymphoid cells

Intestinal lymphoid cells were isolated from the intestine by incubation in 1 mM EDTA/ Ca^{2+} Mg^{2+}-free Hanks medium or in PBS supplemented with 1 mM EDTA, 15 mM HEPES and 10% FCS (1-2 × 20-30 min at 37°C), with gentle shaking to remove intestinal epithelial cells. Supernatants were discarded and tissues were then incubated, with gentle shaking, for 2 × 30 min or 1 × 45 min in 1-1.5 mg/ml (w/v) collagenase type III (Worthington), 200 μg/ml DNase I (Roche), 0.4 units/mL Dispase (Gibco) in mouse tonicity RPMI-1640 + 2% (v/v) FCS, or for 45 min at 37°C in RPMI supplemented with 15 mM HEPES and 300 units/mL collagenase type VIII (Sigma). Preparations were filtered and mononuclear cells were isolated on a 40%/80% or 90/100% Percoll gradient. Lymphocytes were recovered from the interface and washed twice. Mesenteric lymph nodes and splenic lymphoid cells were isolated by mashing organs on filters with 70 μm filters and resuspending the material retained on the filter in PBS supplemented with 1 mM EDTA.

In vitro T cell restimulation

mLN or splenic cells were cultured for 4 hours in complete RPMI in the presence of PMA (200 ng/mL), ionomycin (1 μg/mL) and BD GolgiStop and GolgiPlug (1:1000) (BD Biosciences), for the determination of intracellular cytokines.

Flow cytometry

For surface molecule analyses, cells were stained with antibodies against the following markers: CD19 (clone 1D3), CD3ε (clone 1452C11), NKp46 (clone 29A1.4), CD4 (clone GK1.4), NK1.1 (clone PK136), NKG2A/E/C (clone 20d5), CD94 (clone 18d3), KLRG-1 (clone 2F1), CD11c (clone N418) (from eBioscience), CD45.2 (clone 104), CD117 (clone 2B8), CD8α (clone 53-6.7), (I-A/I-E (clone M5/114.15.2), Ly6-C (clone AL-21), Ly6-G (clone 1A8) (from BD Bioscience) and CD49b (clone DX5, generated at the WEHI hybridoma facility). Live cells were identified by propidium iodide exclusion or with a fixable blue dead cell stain kit (Invitrogen). For intracellular staining, cells were stained for surface markers and with Fixable Viability Dye (eBiosciences), then fixed and permeabilized with either the eBioscience intracellular staining kit or the Cytofix/ Cytoperm™ kit (BD Biosciences). Intracellular staining was then carried out with antibodies against the transcription factors Rorγt (clone Q31-378, BD Biosciences or AFKJS-9, eBiosciences), aand T-bet (clone eBio4B10, eBioscience) or the cytokines IL-22 (clone IL22JOP, eBioscience or kindly provided by JC Renauld; antibody coupled to Alexa Fluor

647 with the antibody labeling kit from Life Technologies), IFN-γ (clone XMG1.2) and IL-17A (clone TC11-18h10) (BD Bioscience). IL-22 production was induced in cells by stimulation with IL-23 (10-40 ng/ml) for 4-5 hours in the presence of BD GolgiStop™ and BD GolgiPlug™ (1:1000) (BD Biosciences) in complete RPMI-1640 medium (containing 10% FCS, 50 mM 2-mercaptoethanol, 1 mM L-glutamine, 100 U/ml penicillin and 100 µg/ml streptomycin) at 37°C. Flow cytometry was performed with a CantoII™, LSRFortessa™ X-20 or LSR-II cytometer (BD Biosciences) and FlowJo analysis software (Freestar).

Cell purification

Small intestinal lamina propria lymphocytes (pooled from 3-6 mice) were stained with surface antibodies and cells were purified with a BD FACSAria™ cell sorter (BD Biosciences). Cells were sorted into 50% v/v FCS/PBS or the appropriate cell culture medium in tubes previously coated with heat-inactivated FCS.

mRNAseq analysis

Total RNA for RT-quantitative PCR was prepared from purified ILC populations with an RNeasy mini kit (Qiagen). We generated cDNA from total RNA with OligodT primers and the Thermoscript reverse transcriptase (Invitrogen). Quantitative PCR was then performed with the SensiMix SYBR no-Rox kit (Bioline). Approximately 5×10^5 lin^- ($CD3^-CD19^-$) $CD45.2^+$ cells from each ILC subset were sorted from the intestines of *Rorc*$^{GFP/+}$ and *Rorc*$^{GFP/+}$ *Tbx21*$^{+/-}$ mice and two biological replicates were generated and subjected to 50 bp single-end sequencing on an Illumina HiSeq2000 at the Australian Genome Research Facility (Melbourne, Australia). More than 30 million reads were generated for each replicate and aligned with the GRCm38/mm10 build of the *Mus musculus* genome, using the Subread aligner [46]. Genewise counts were obtained with featureCounts [47]. Reads overlapping exons in annotation build 38.1 of the NCBI RefSeq database were included. Genes were filtered out and excluded from downstream analysis if they failed to achieve a CPM (counts per million mapped reads) value of at least 0.5 in at least two libraries. Counts were converted to log2 counts per million, quantile-normalized and precision-weighted with the voom function of the limma package [48]. A linear model was fitted to each gene [49] and empirical Bayes moderated t-statistics were used to assess differences in expression [50]. Genes were called differentially expressed if they achieved a false discovery rate of <= 0.1 and an average RPKM (reads per kilobase per million) of >= 8 in at least one of the two groups being compared.

Histology

Colons were gently flushed clean and cut into three sections, corresponding to the proximal, mid and distal colon. Alternatively, colons were cut longitudinally, cleaned and formed into a ‘Swiss’ roll, to visualize the full length of the colon on sectioning. The cecum was opened along the mesenteric side and its contents cleaned. Tissues were fixed in 10% neutral buffered formalin and processed for wax embedding and routine hematoxylin and eosin (H&E) staining. The ceca were sectioned longitudinally, parallel to the mesenteric axis. Images were collected and analyzed with Aperio™ ImageScope v11.2.0.780 software. Colitis severity was assessed blind, by determining a combined score of immune cell

infiltration and epithelial damage based on hyperproliferation, crypt loss and the presence of ulcers (Supplementary Table 3).

Colon homogenates

Explants of distal colon were isolated, weighed and cut. They were then homogenized in 2 mL of complete RPMI 1640 medium (as previously described) and incubated for 24 h at 37°C. The supernatants were collected for cytokine measurement.

Cytokine measurement

Levels of IFN-γ, IL-17A, TNFα, IL-6, IL-1β, KC and IL-10 were assessed with a cytometric bead array (BD Bioscience), according to the manufacturer's protocol.

Microbiota sequencing

Fresh mouse stool samples were collected and immediately stored at −80°C. DNA was extracted from stools, and its quality and quantity were checked with NanoDrop and Qubit, together with the BR assay. Barcoding PCR was carried out with indexed primers targeting the V3-V5 of the 16S rRNA gene. AccuPrime™ Pfx SuperMix (Invitrogen - 12344-040) was used for PCR. The PCR mix consisted of 18 µL of AccuPrime™ Pfx SuperMix, 0.5 µL of both the V3-340F and V5-926R primers (0.2 µM) and 1 µL of DNA (10 ng). PCR was carried out as follows: 95°C for 2 min, 30 cycles of 95°C for 20 s, 55°C for 15 s, 72°C for 5 min and a final extension step at 72°C for 10 min. PCR products were then quantified with the Qubit BR DNA assay kit. Equal amounts of each PCR mixture were pooled and thoroughly mixed. The amplicon pool was then loaded on an agarose gel (1.5%) and subjected to electrophoresis for 45 min at 100 V. The band corresponding to V3-V5 of the 16S rDNA amplicon was extracted from the gel and purified with the Qiaquick gel extraction kit (Qiagen - 28704). Amplicon quantity and integrity were checked by agarose gel electrophoresis and with the Qubit BR DNA assay kit. The amplicon was stored at −20°C until use. The 16S rDNA amplicon library was sequenced at the Institut Curie NGS platform, on a MiSeq machine, with the 2*300 bp V3 kit. Reads was merged with FLASH and trimmed with an in-house analysis script (length ≥ 500 bp, quality ≥ 25). Reads were clustered at 97% identity with the vsearch pipeline (http://zenodo.org/record/15524#.VPIujy4f2J8). Chimeric OTU were identified with UCHIME and discarded from subsequent analysis. The taxonomy of representative OTU sequences was determined with RDP classifier. OTU sequences were aligned, using ssu-align. The phylogenetic tree was inferred from multiple alignments of the OTUs generated with Fattree2. Statistical analyses were performed with R software (R Development Core Team 2012) and various related packages (Ade4,Vegan, ape, phyloseq). Weighted unifrac distances were calculated from a microbiota abundance table and phylogenetic tree. Statistical tests were performed with the Wilcoxon test (p-value). The false discovery rate method was used to correct for multiple testing (q-value).

SFB quantification

Mice were housed by genotype, and feces were collected at the ages of 10 and 15 weeks. The protocol for DNA extraction was adapted from the RBB+C method described by

Zhongtang Yu and Mark Morrison, 2004. In brief, feces were homogenized in lysis buffer, using FASTprep. DNA was precipitated in ammonium acetate and washed with 70% ethanol. For the removal of RNA and protein, samples were further purified with the DNeasy Blood and Tissue Kit from Qiagen. Standard SYBRGreen qPCR was performed. Total bacteria detection was carried out with primers 1369f (5'-CGG TGA ATA CGT TCC CGG-3') and 1492r (5'-TAC GGC TAC CTT GTT ACG ACT T-3'); SFB were detected with primers 779f (5'-TGTGGGTTGTGAATAACAAT-3') and 1008r (5'-GCGGGCTTCCCTCATTACAAGG-3'). DNA from the feces of SFB single-colonized mice was used as a control for calculation of the relative amount of SFB by the Pfaffl-Method: Ratio= 〖(E_target)〗^(ΔCT,target (calibrator-test))/ 〖(E_ref)〗^(ΔCT,ref (calibrator-test)).

Statistical analysis

All statistical analyses were performed with GraphPad Prism version 6.0d (Graphpad Software, San Diego, California, USA). We used unpaired two-tailed Student's *t*-tests for pairwise comparisons. Unpaired and paired Student's *t*-tests, nonparametric Mann-Whitney or Log-rank Mantel-Cox tests were used, as indicated. The data shown are the mean ± standard deviation (SD) or mean ± standard error of mean (SEM) as indicated in figure legends. *P < 0.05, **P < 0.01, ***P < 0.001 and ****P < 0.0001 throughout.

Supplementary Material

Refer to Web version on PubMed Central for supplementary material.

ACKNOWLEDGMENTS

This work was supported by grants and fellowships from the National Health and Medical Research Council (NHMRC) of Australia (G.T.B., S.C., N.H.) a NHMRC Dora Lush Postgraduate Research Scholarship (L.R); ARC Future Fellowships (J.R.G. and G.T.B.); We thank M. Camilleri, J. Vella, E. Loza and L. Inglis and the staff of the animal and flow cytometry facilities of WEHI and CIML for technical assistance; and Dr Susan Kaech (Yale), who kindly provided T-bet floxed mice. The E.V. laboratory members also thank L. Chasson and C. Laprie for providing expertise in histology and for the blind scoring of sections. This work was made possible through Victorian State Government Operational Infrastructure Support and Australian Government NHMRC IRIIS. The EV laboratory is supported by the European Research Council (THINK Advanced Grant), the *Ligue Nationale contre le Cancer (Equipe Labellisée)* and by institutional grants from INSERM, CNRS and Aix-Marseille University to CIML. E.V. is a scholar of the *Institut Universitaire de France*.

REFERENCES

1. Dudakov JA, Hanash AM, van den Brink MR. Interleukin-22: Immunobiology and Pathology. Annu Rev Immunol. 2015; 33:747–85. [PubMed: 25706098]
2. Spits H, Artis D, Colonna M, Diefenbach A, Di Santo JP, Eberl G, et al. Innate lymphoid cells--a proposal for uniform nomenclature. Nat Rev Immunol. 2013; 13:145–149. [PubMed: 23348417]
3. McKenzie AN, Spits H, Eberl G. Innate lymphoid cells in inflammation and immunity. Immunity. 2014; 41:366–374. [PubMed: 25238094]
4. Diefenbach A, Colonna M, Koyasu S. Development, differentiation, and diversity of innate lymphoid cells. Immunity. 2014; 41:354–365. [PubMed: 25238093]
5. Montaldo E, Juelke K, Romagnani C. Group 3 innate lymphoid cells (ILC3s): Origin, differentiation, and plasticity in humans and mice. Eur J Immunol. 2015; 45:2171–2182. [PubMed: 26031799]
6. Eberl G, Di Santo JP, Vivier E. The brave new world of innate lymphoid cells. Nat Immunol. 2015; 16:1–5. [PubMed: 25521670]

7. Eberl G, Colonna M, Di Santo JP, McKenzie AN. Innate lymphoid cells: a new paradigm in immunology. Science. 2015; 348:aaa6566. [PubMed: 25999512]

8. Mebius RE, Rennert P, Weissman IL. Developing lymph nodes collect $CD4^+CD3^-$ $LTbeta^+$ cells that can differentiate to APC, NK cells, and follicular cells but not T or B cells. Immunity. 1997; 7:493–504. [PubMed: 9354470]

9. Constantinides MG, Gudjonson H, McDonald BD, Ishizuka IE, Verhoef PA, Dinner AR, et al. PLZF expression maps the early stages of ILC1 lineage development. Proc Natl Acad Sci USA. 2015; 112:5123–5128. [PubMed: 25838284]

10. Klose CS, Kiss EA, Schwierzeck V, Ebert K, Hoyler T, d'Hargues Y, et al. A T-bet gradient controls the fate and function of CCR6-RORgammat+ innate lymphoid cells. Nature. 2013; 494:261–265. [PubMed: 23334414]

11. Rankin LC, Groom JR, Chopin M, Herold MJ, Walker JA, Mielke LA, et al. The transcription factor T-bet is essential for the development of NKp46+ innate lymphocytes via the Notch pathway. Nat Immunol. 2013; 14:389–395. [PubMed: 23455676]

12. Kirchberger S, Royston DJ, Boulard O, Thornton E, Franchini F, Szabady RL, et al. Innate lymphoid cells sustain colon cancer through production of interleukin-22 in a mouse model. J Exp Med. 2013; 210:917–931. [PubMed: 23589566]

13. Satoh-Takayama N, Vosshenrich CA, Lesjean-Pottier S, Sawa S, Lochner M, Rattis F, et al. Microbial flora drives interleukin 22 production in intestinal NKp46+ cells that provide innate mucosal immune defense. Immunity. 2008; 29:958–970. [PubMed: 19084435]

14. Cella M, Fuchs A, Vermi W, Facchetti F, Otero K, Lennerz JK, et al. A human natural killer cell subset provides an innate source of IL-22 for mucosal immunity. Nature. 2009; 457:722–725. [PubMed: 18978771]

15. Sonnenberg GF, Fouser LA, Artis D. Functional Biology of the IL-22-IL-22R Pathway in Regulating Immunity and Inflammation at Barrier Surfaces. Adv Immunol. 2010; 107:1–29. [PubMed: 21034969]

16. Zheng Y, Valdez PA, Danilenko DM, Hu Y, Sa SM, Gong Q, et al. Interleukin-22 mediates early host defense against attaching and effacing bacterial pathogens. Nat Med. 2008; 14:282–289. [PubMed: 18264109]

17. Satoh-Takayama N, Serafini N, Verrier T, Rekiki A, Renauld JC, Frankel G, et al. The chemokine receptor CXCR6 controls the functional topography of interleukin-22 producing intestinal innate lymphoid cells. Immunity. 2014; 41:776–788. [PubMed: 25456160]

18. Artis D, Spits H. The biology of innate lymphoid cells. Nature. 2015; 517:293–301. [PubMed: 25592534]

19. van de Pavert SA, Vivier E. Differentiation and function of group 3 innate lymphoid cells, from embryo to adult. Int Immunol. 2015:pii: dxv052. [PubMed: 26374472]

20. Robinette ML, Fuchs A, Cortez VS, Lee JS, Wang Y, Durum SK, et al. Transcriptional programs define molecular characteristics of innate lymphoid cell classes and subsets. Nat Immunol. 2015; 16:306–317. [PubMed: 25621825]

21. Sciume G, Hirahara K, Takahashi H, Laurence A, Villarino AV, Singleton KL, et al. Distinct requirements for T-bet in gut innate lymphoid cells. J Exp Med. 2012; 209:2331–2338. [PubMed: 23209316]

22. Guo X, Qiu J, Tu T, Yang X, Deng L, Anders RA, et al. Induction of innate lymphoid cell-derived interleukin-22 by the transcription factor STAT3 mediates protection against intestinal infection. Immunity. 2014; 40:25–39. [PubMed: 24412612]

23. Sathe P, Delconte RB, Souza-Fonseca-Guimaraes F, Seillet C, Chopin M, Vandenberg CJ, et al. Innate immunodeficiency following genetic ablation of Mcl1 in natural killer cells. Nature communications. 2014; 5:4539.

24. Qiu J, Guo X, Chen ZM, He L, Sonnenberg GF, Artis D, et al. Group 3 innate lymphoid cells inhibit T-cell-mediated intestinal inflammation through aryl hydrocarbon receptor signaling and regulation of microflora. Immunity. 2013; 39:386–399. [PubMed: 23954130]

25. Guo X, Liang Y, Zhang Y, Lasorella A, Kee BL, Fu YX. Innate lymphoid cells control early colonization resistance against intestinal pathogens through ID2-dependent regulation of the microbiota. Immunity. 2015; 42:731–743. [PubMed: 25902484]

26. Basu R, O'Quinn DB, Silberger DJ, Schoeb TR, Fouser L, Ouyang W, et al. Th22 cells are an important source of IL-22 for host protection against enteropathogenic bacteria. Immunity. 2012; 37:1061–1075. [PubMed: 23200827]

27. Ahlfors H, Morrison PJ, Duarte JH, Li Y, Biro J, Tolaini M, et al. IL-22 fate reporter reveals origin and control of IL-22 production in homeostasis and infection. J Immunol. 2014; 193:4602–4613. [PubMed: 25261485]

28. Vonarbourg C, Mortha A, Bui VL, Hernandez PP, Kiss EA, Hoyler T, et al. Regulated Expression of Nuclear Receptor RORgammat Confers Distinct Functional Fates to NK Cell Receptor-Expressing RORgammat(+) Innate Lymphocytes. Immunity. 2010; 33:736–751. [PubMed: 21093318]

29. Dhiman R, Indramohan M, Barnes PF, Nayak RC, Paidipally P, Rao LV, et al. IL-22 produced by human NK cells inhibits growth of Mycobacterium tuberculosis by enhancing phagolysosomal fusion. J Immunol. 2009; 183:6639–6645. [PubMed: 19864591]

30. Guo H, Topham DJ. Interleukin-22 (IL-22) production by pulmonary Natural Killer cells and the potential role of IL-22 during primary influenza virus infection. J Virol. 2010; 84:7750–7759. [PubMed: 20504940]

31. Male V, Hughes T, McClory S, Colucci F, Caligiuri MA, Moffett A. Immature NK cells, capable of producing IL-22, are present in human uterine mucosa. J Immunol. 2010; 185:3913–3918. [PubMed: 20802153]

32. Tang Q, Ahn YO, Southern P, Blazar BR, Miller JS, Verneris MR. Development of IL-22-producing NK lineage cells from umbilical cord blood hematopoietic stem cells in the absence of secondary lymphoid tissue. Blood. 2011; 117:4052–4055. [PubMed: 21310921]

33. Xu X, Weiss ID, Zhang HH, Singh SP, Wynn TA, Wilson MS, et al. Conventional NK cells can produce IL-22 and promote host defense in Klebsiella pneumoniae pneumonia. J Immunol. 2014; 192:1778–1786. [PubMed: 24442439]

34. Macho-Fernandez E, Koroleva EP, Spencer CM, Tighe M, Torrado E, Cooper AM, et al. Lymphotoxin beta receptor signaling limits mucosal damage through driving IL-23 production by epithelial cells. Mucosal Immunol. 2015; 8:403–413. [PubMed: 25183367]

35. Sonnenberg GF, Monticelli LA, Alenghat T, Fung TC, Hutnick NA, Kunisawa J, et al. Innate lymphoid cells promote anatomical containment of lymphoid-resident commensal bacteria. Science. 2012; 336:1321–1325. [PubMed: 22674331]

36. Sonnenberg GF, Monticelli LA, Elloso MM, Fouser LA, Artis D. CD4(+) lymphoid tissue-inducer cells promote innate immunity in the gut. Immunity. 2011; 34:122–134. [PubMed: 21194981]

37. Hepworth MR, Monticelli LA, Fung TC, Ziegler CG, Grunberg S, Sinha R, et al. Innate lymphoid cells regulate CD4+ T-cell responses to intestinal commensal bacteria. Nature. 2013; 498:113–117. [PubMed: 23698371]

38. Gasteiger G, Rudensky AY. Interactions between innate and adaptive lymphocytes. Nat Rev Immunol. 2014; 14:631–639. [PubMed: 25132095]

39. Wiles S, Clare S, Harker J, Huett A, Young D, Dougan G, et al. Organ specificity, colonization and clearance dynamics in vivo following oral challenges with the murine pathogen Citrobacter rodentium. Cell Microbiol. 2004; 6:963–972. [PubMed: 15339271]

40. Smith HF, Fisher RE, Everett ML, Thomas AD, Bollinger RR, Parker W. Comparative anatomy and phylogenetic distribution of the mammalian cecal appendix. J. Evol. Biol. 2009; 22:1984–1999. [PubMed: 19678866]

41. Frisch M, Pedersen BV, Andersson RE. Appendicitis, mesenteric lymphadenitis, and subsequent risk of ulcerative colitis: cohort studies in Sweden and Denmark. Bmj. 2009; 338:b716. [PubMed: 19273506]

42. Alonzi T, Maritano D, Gorgoni B, Rizzuto G, Libert C, Poli V. Essential role of STAT3 in the control of the acute-phase response as revealed by inducible gene inactivation [correction of activation] in the liver. Mol Cell Biol. 2001; 21:1621–1632. [PubMed: 11238899]

43. Eberl M, Jomaa H, Hayday AC. Integrated immune responses to infection - cross-talk between human gammadelta T cells and dendritic cells. Immunology. 2004; 112:364–368. [PubMed: 15196203]

44. Nieuwenhuis EE, Neurath MF, Corazza N, Iijima H, Trgovcich J, Wirtz S, et al. Disruption of T helper 2-immune responses in Epstein-Barr virus-induced gene 3-deficient mice. Proc Natl Acad Sci USA. 2002; 99:16951–16956. [PubMed: 12482940]

45. Narni-Mancinelli E, Chaix J, Fenis A, Kerdiles YM, Yessaad N, Reynders A, et al. Fate mapping analysis of lymphoid cells expressing the NKp46 cell surface receptor. Proc Natl Acad Sci USA. 2011; 108:18324–18329. [PubMed: 22021440]

46. Thakur C, Lu Y, Sun J, Yu M, Chen B, Chen F. Increased expression of mdig predicts poorer survival of the breast cancer patients. Gene. 2014; 535:218–224. [PubMed: 24309373]

47. Liao Y, Smyth GK, Shi W. featureCounts: an efficient general purpose program for assigning sequence reads to genomic features. Bioinformatics. 2014; 30:923–930. [PubMed: 24227677]

48. Ritchie ME, Phipson B, Wu D, Hu Y, Law CW, Shi W, et al. limma powers differential expression analyses for RNA-sequencing and microarray studies. Nucleic acids research. 2015; 43:e47. [PubMed: 25605792]

49. Smyth GK. Linear models and empirical bayes methods for assessing differential expression in microarray experiments. Stat Appl Genet Mol Biol. 2004; 3 Article3.

50. McCarthy DJ, Smyth GK. Testing significance relative to a fold-change threshold is a TREAT. Bioinformatics. 2009; 25:765–771. [PubMed: 19176553]

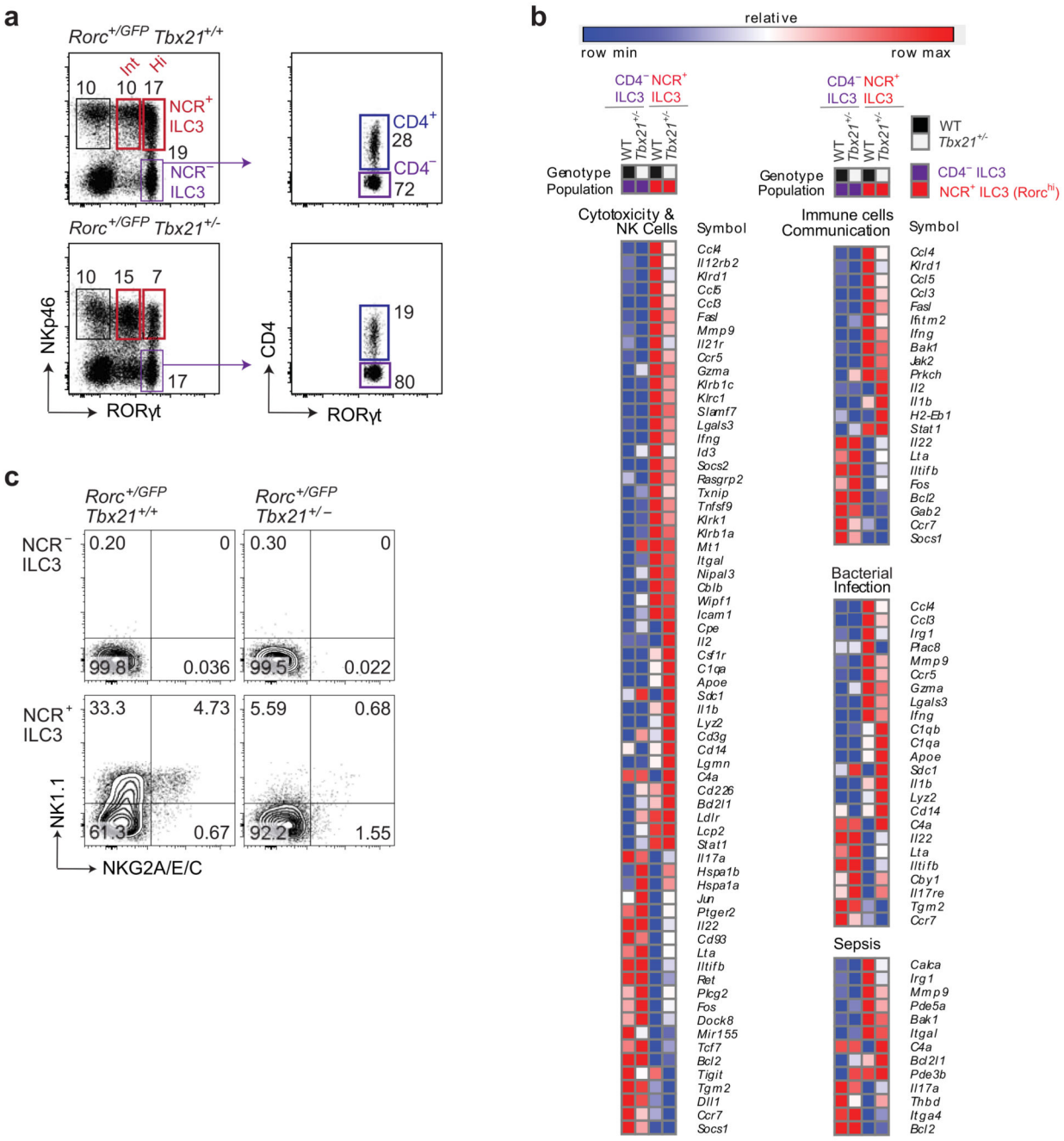

Figure 1. RNAseq analysis of ILC3 subsets

(a) Sorting strategy for RNAseq analyses of ILC3 subsets isolated from the small intestine of *Rorc*$^{gfp/+}$ *Tbx21*$^{+/+}$ (wild-type) after gating on live CD45$^+$ lin$^-$(CD3$^-$CD19$^-$) cells (left plot). CD4$^+$ NKp46$^-$ RORγt$^+$ and CD4$^-$NKp46$^-$ RORγt$^+$ segregated among NCR$^-$ ILC3 (right plot).

(b) Analyses of gene clusters regulated by T-bet between *Tbx21*$^{+/+}$ and *Tbx21*$^{+/-}$ NCR$^+$ ILC3 at steady state. Ingenuity pathway analysis (IPA) was carried out for genes differentially expressed between NCR$^-$ and NCR$^+$ ILC3 affected by the loss of a single copy

of T-bet. Significant enrichment was observed for several pathways, grouped into three main categories: cytotoxicity & NK cells, immune cell communication and infectious disease. The expression values for the genes of these enriched pathways were converted into heat maps, using the mean and maximum values for each gene (Log2 reads per kilobase of transcript per million reads, RPKM).

(c) Flow cytometry analyses of NK1.1 and NKG2A/E/C protein levels in the indicated ILC3 subsets isolated from the intestines of *Rorc*$^{GFP/+}$ *Tbx21*$^{+/+}$ and *Rorc*$^{GFP/+}$ *Tbx21*$^{+/-}$ mice. Plots are gated on live CD45^{+}lin^{-} RORγt^{+} cells and show one representative experiment. Numbers show the frequency of NCR^{+} ILC3 in the indicated quadrants. Plots show representative results from two independent experiments (n = 2-3 mice per genotype per experiment).

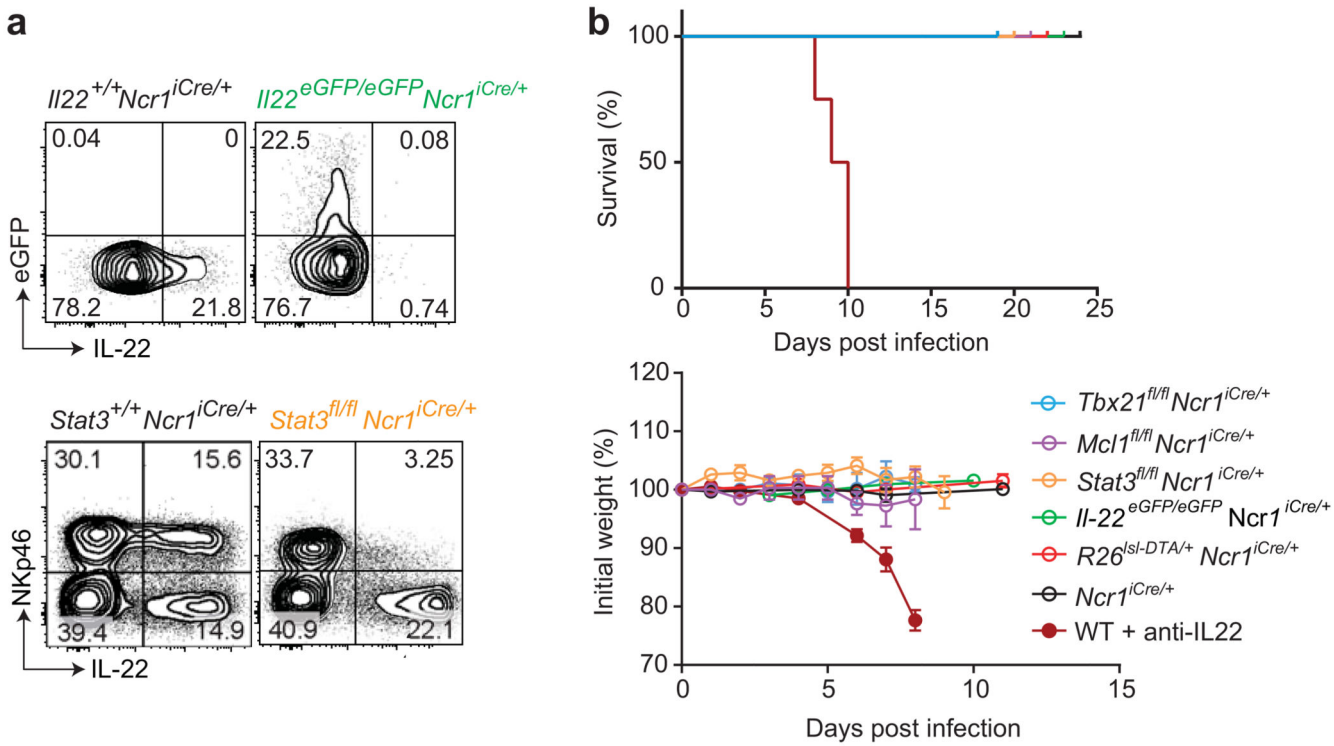

Figure 2. Targeting of NCR$^+$ ILC3 during *C. rodentium* infection

(a) Upper panels show the production of IL-22 by small intestine Lin$^-$CD45$^+$NCR$^+$ ILC3 from naive *Il22*$^{eGFP/eGFP}$*Ncr1*-iCre and control mice upon *in vitro* stimulation with IL-23 for 4-5 h in the presence of brefeldin A. The lower panels show the frequency of IL-22-producing cells among the NKp46$^+$ and NKp46$^-$ cells gated on Lin$^-$CD45.2$^+$ small intestine lymphocytes from *Stat3*$^{fl/fl}$*Ncr1*$^{+/+}$*Rorc*$^{GFP/+}$ and *Stat3*$^{fl/fl}$*Ncr1*-iCre*Rorc*$^{GFP/+}$ mice 8 days after *C. rodentium* infection. Cells were stimulated *in vitro* with IL-23 for 4-5 hr in the presence of brefeldin A to elicit IL-22 production. Data show representative plots from one of two independent experiments (n = 3-4 mice per genotype per experiment).

(b) Survival curve and change in body weight of indicated mice and *Ncr1*$^{iCre/+}$ controls following *C. rodentium* infection. In addition, WT mice were treated with anti-IL-22 blocking mAbs twice weekly, beginning on day -1. Pooled data from independent experiments are shown. The data shown are means ± SEM.

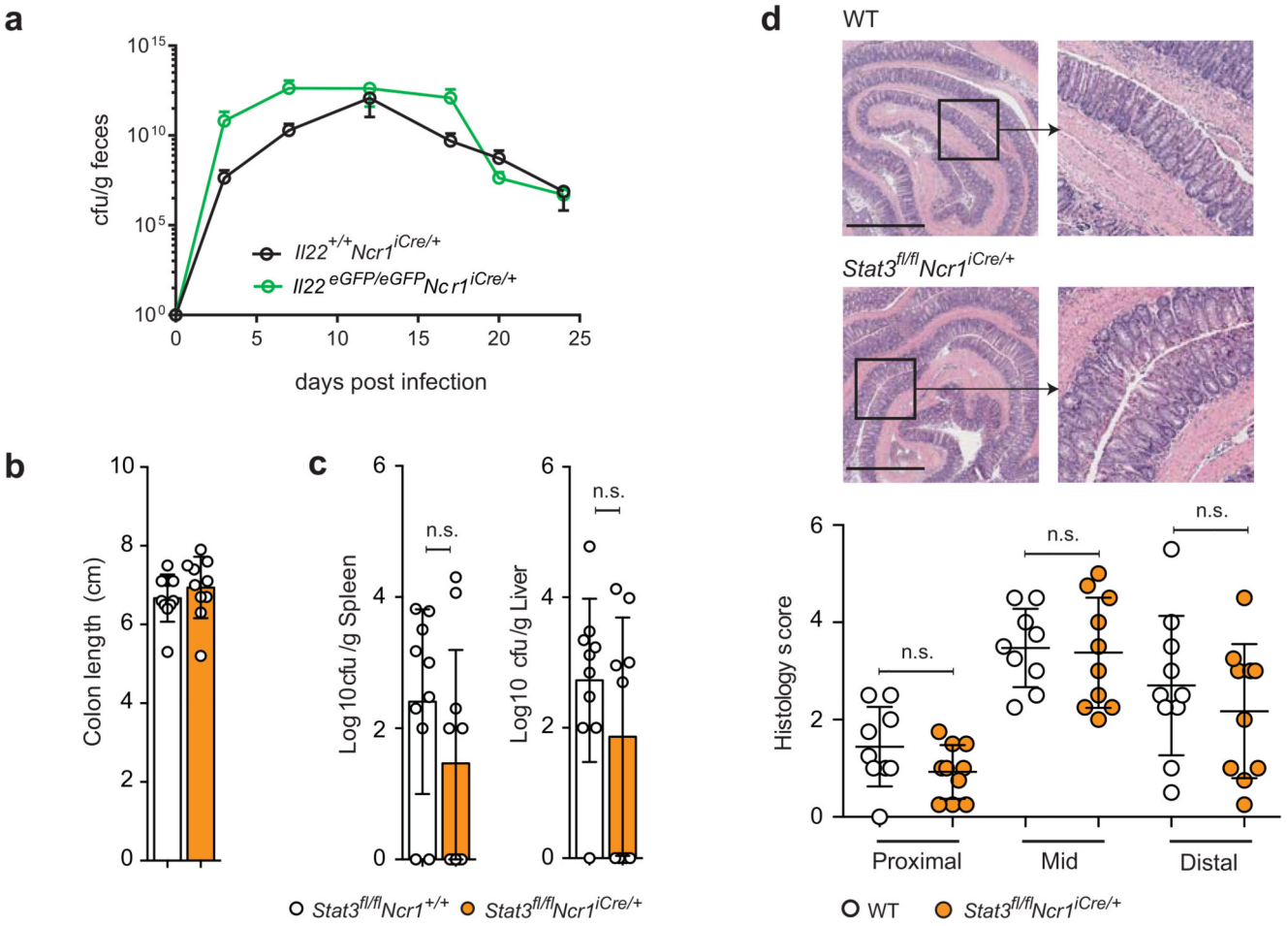

Figure 3. *C. rodentium* infection in the absence of IL-22 production by NCR$^+$ ILC3
(a) *Il22*$^{eGFP/eGFP}$*Ncr1*-iCre mice and controls were orally inoculated with 10^{10} cfu *C. rodentium* on day 0. Counts of *C. rodentium* (cfu) in the feces are shown as a function of time post-infection. Data shown are from one out of three independent experiments (n = 4-6 mice per group per experiment). Shown are means ± SD.
(b-d) Male *Stat3*$^{fl/fl}$*Ncr1*$^{+/+}$ and *Stat3*$^{fl/fl}$*Ncr1*-iCre mice were orally inoculated with 2×10^9 cfu of *C. rodentium.* **(b)** Colon length of the indicated mice 8 days after infection. Data were pooled from three independent experiments (n = 3-4 mice per group per experiment). **(c)** Bacterial loads (cfu/g) were measured 8 days post-infection (liver and spleen). **(d)** Pathological features in the colon of the indicated mice 8 days after infection. Representative H&E staining of formalin-fixed paraffin-embedded sections (micrographs) of colons and blinded histological scoring (see Supplementary Table 3). The scale bar represents 1000 µm and the insets are × 3.4 magnifications. Data were pooled from three independent experiments (n = 3-4 mice per group per experiment). The data shown are means ± SD. Statistical analyses was performed with unpaired Student's *t*-tests; n.s., not statistically significant.

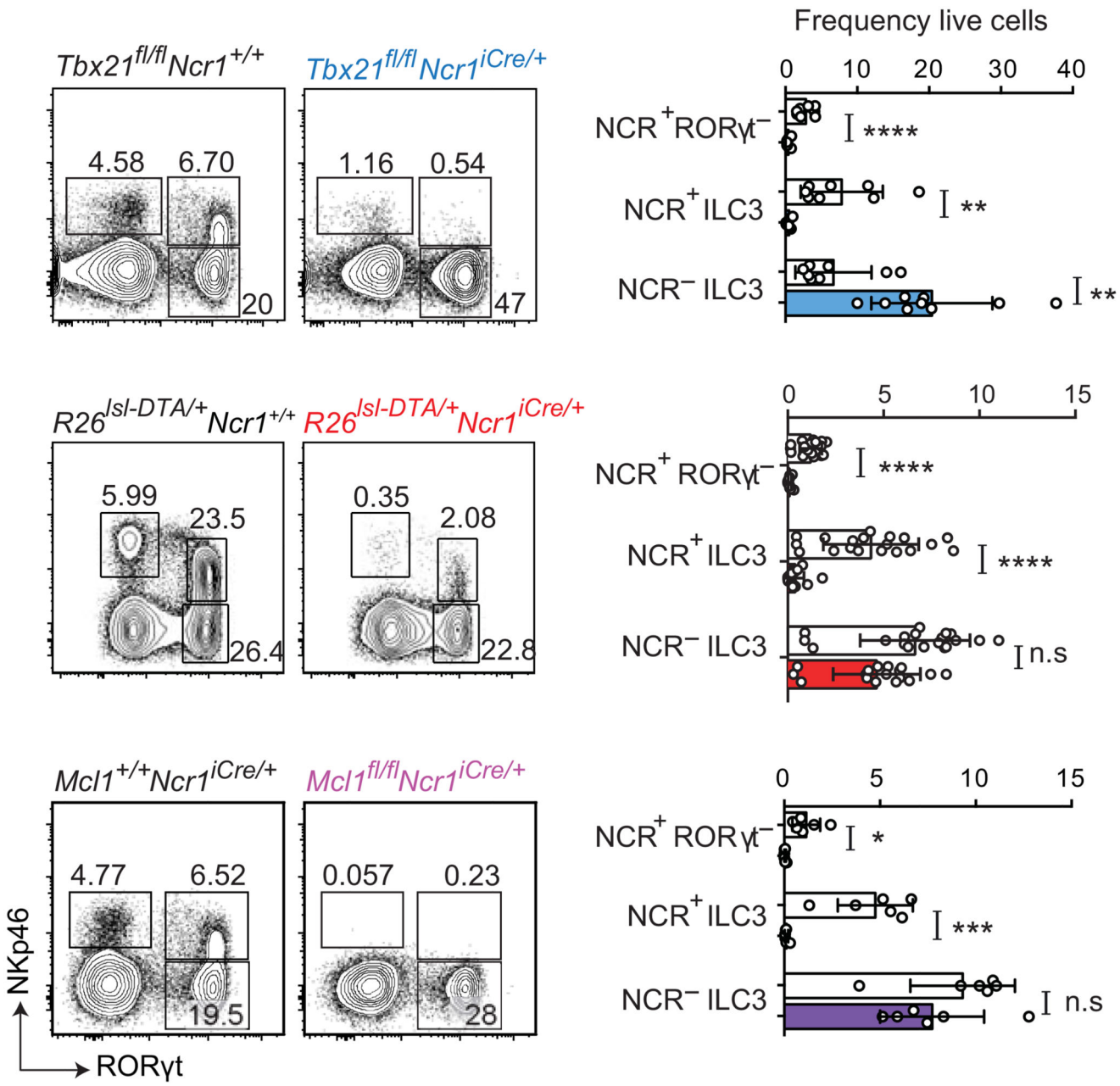

Figure 4. Impact of *Tbx21* and *Mcl1* deletion or *DTA* expression on NCR$^+$ ILC3
Analysis of Lin$^-$CD45$^+$ small intestinal lymphocytes from naive *Tbx21*$^{fl/fl}$*Ncr1*$^{iCre/+}$, *R26*$^{DTA/+}$*Ncr1*-iCre and *Mcl1*$^{fl/fl}$*Ncr1*-iCre mice and their respective controls. Flow cytometry plots show intracellular RORγt and surface NKp46 expression. Numbers show the frequency of cells within the indicated gate. Data are pooled from at least three independent experiments (n = 2-4 mice per group per experiment) and the mean ± SD is shown. Statistical analyses were performed with unpaired Student's t-tests. n.s., not statistically significant. *P < 0.05, **P < 0.01, ***P < 0.001 and ****P < 0.0001.

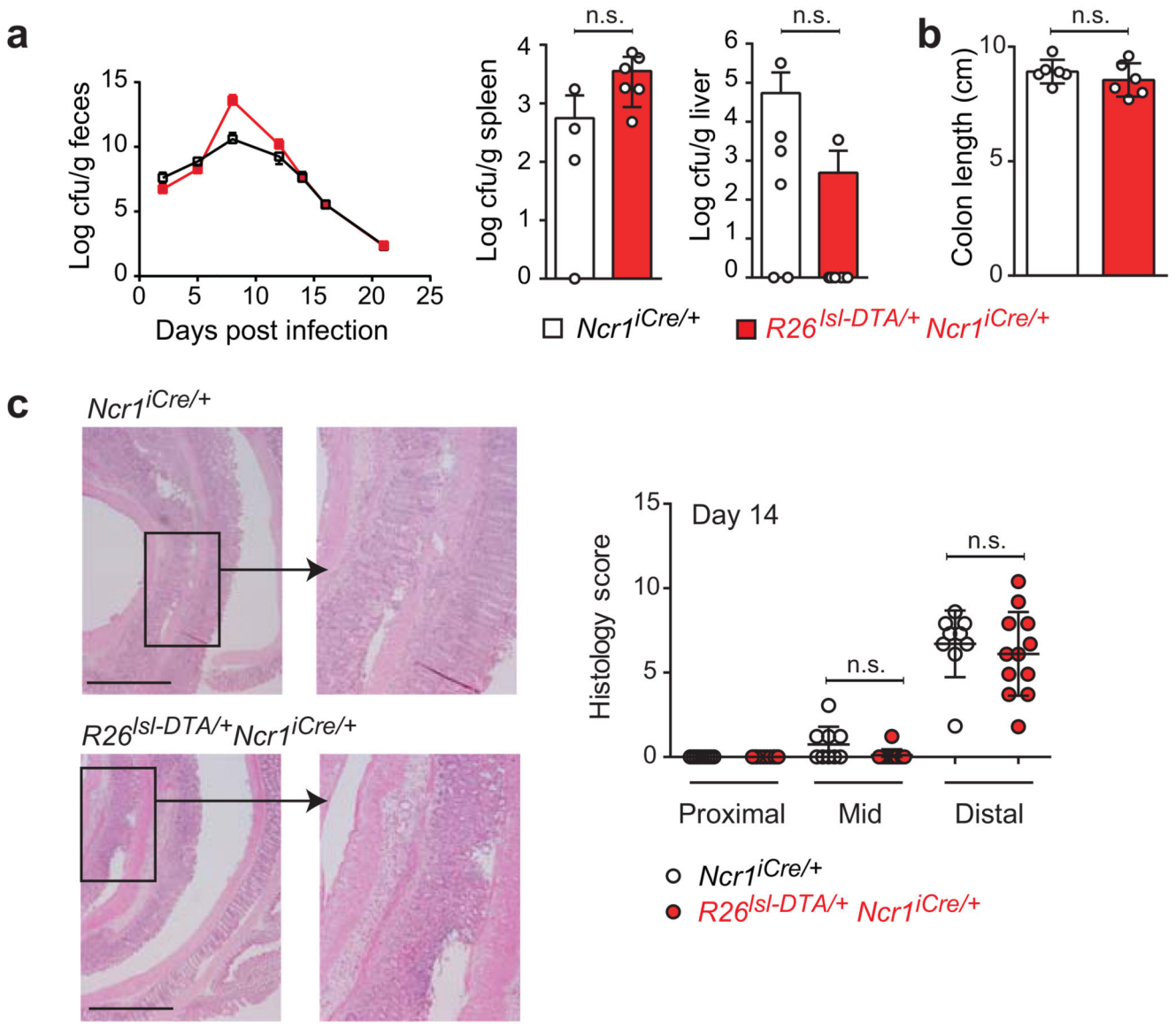

Figure 5. *C. rodentium* infection in the absence of NCR$^+$ ILC3

R26$^{DTA/+}$*Ncr1*-iCre and *Ncr1*-iCre littermates were orally inoculated with 10^{10} cfu *C. rodentium* on day 0. (**a**) Bacterial loads (cfu/g) were determined over the course of the experiment (feces) and at 14 days post-infection (liver and spleen). The data shown are representative of three independent experiments (n = 4-8 mice per group). (**b**) Colon length and **(c)** pathological features, for *R26*$^{DTA/+}$*Ncr1*-iCre and *Ncr1*-iCre controls, 14 days after infection. H&E staining of formalin-fixed paraffin-embedded sections (micrographs) and histological scoring (scatter plots) of colons are shown. The scale bar represents 1000 µm and the insets are x 3.4 magnifications. Histological scores for colon damage were determined on 1- 2 H&E sections per mouse. Data are pooled from two to three independent experiments (n = 4-9 mice/genotype). Statistical analyses were performed with unpaired Student's t-tests. n.s., not statistically significant.

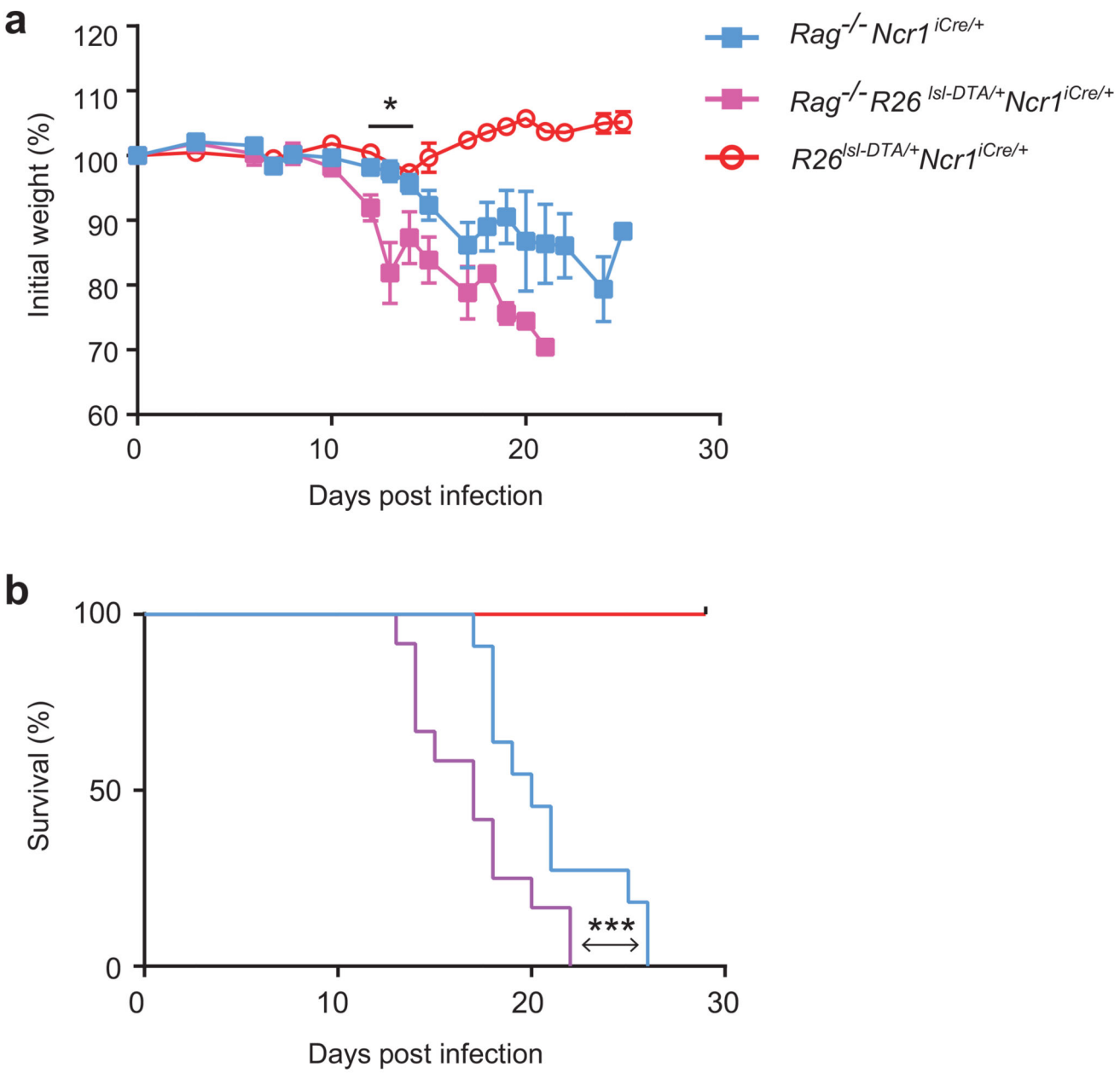

Figure 6. Role of NCR^{+} ILC3 during *C. rodentium* infection in immunocompetent and immunodeficient hosts

Change in body weight (**a**) and survival curves (**b**) of *Rag2*$^{-/-}$*Ncr1*-iCre mice, *Rag2*$^{-/-}$ *R26*$^{DTA/+}$*Ncr1*-iCre and *R26*$^{DTA/+}$*Ncr1*-iCre littermates following *C. rodentium* infection. Data are pooled from 2 independent experiments (n = 3-11 mice per genotype in total). In **(a)**, the data shown are the means ± SEM, * P < 0.04 in unpaired Student's *t*-tests comparing *Rag2*$^{-/-}$ *R26*$^{DTA/+}$*Ncr1*-iCre and *R26*$^{DTA/+}$*Ncr1*-iCre mice at day 12, 13 and 14 post-infection. In **(b)**, statistical analysis was performed with Log-rank Mantel-Cox test, *** P < 0.001.

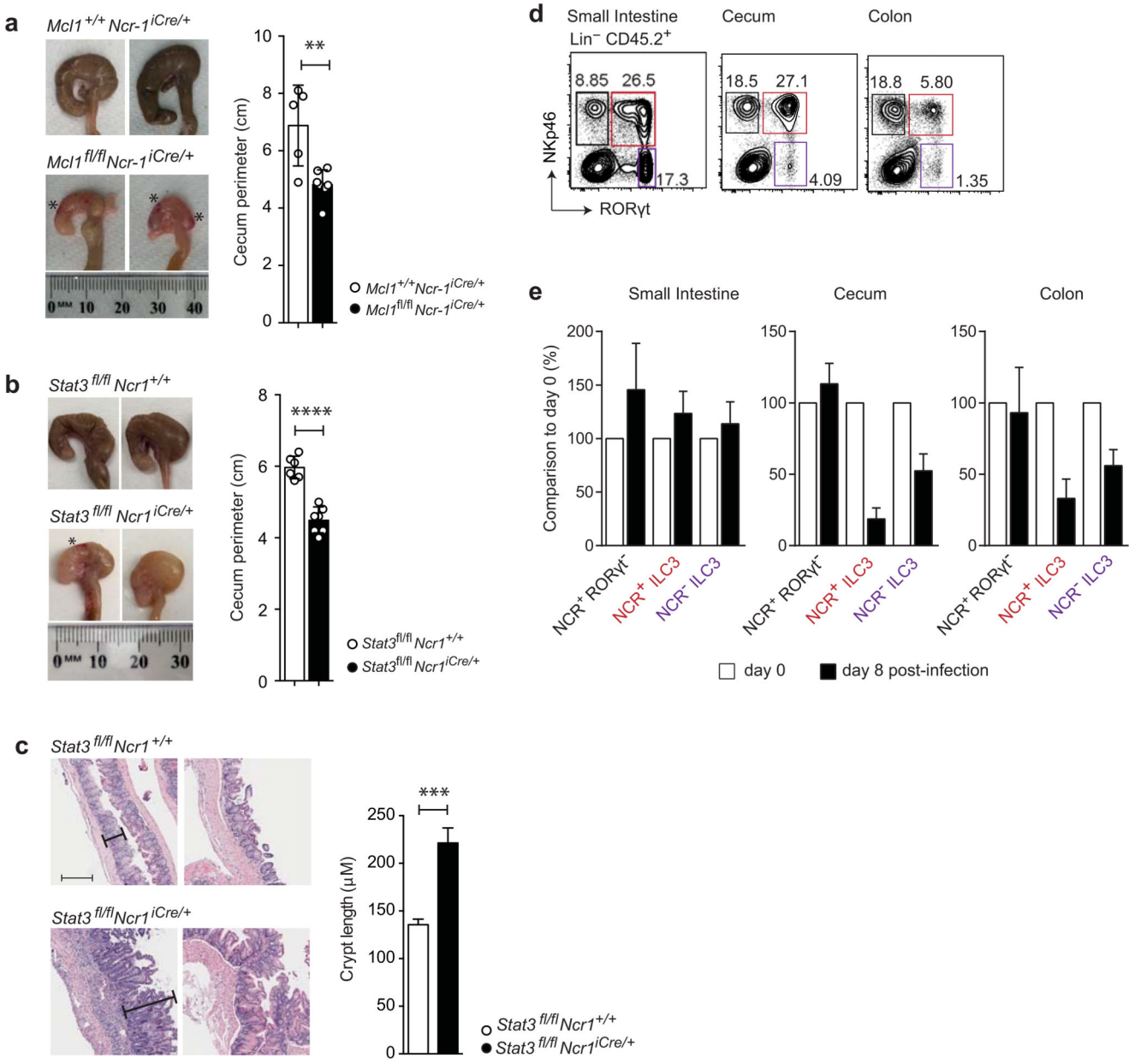

Figure 7. Role of NCR$^+$ ILC3 in cecum homeostasis during *C. rodentium* infection

(a) Representative images of wild-type and *Mcl1*$^{fl/fl}$*Ncr1*-iCre ceca 8 days after infection with 2 × 10^9 cfu *C. rodentium*. * indicates bleeding (left). Cecum size was determined by measuring the perimeter of the organ along the antimesenteric to mesenteric borders. The histogram shows data pooled from two independent experiments (*n*=2-4 mice per genotype per experiment).

(b) Representative images of wild-type and *Stat3*$^{fl/fl}$*Ncr1*-iCre ceca 8 days after infection with 2 × 10^9 cfu *C. rodentium*. * shows bleeding. Cecum size was determined by measuring the perimeter of the organ along the antimesenteric to mesenteric borders. The histogram shows data pooled from two independent experiments (*n* = 3-4 mice per genotype per

experiment). (**a, b)** The data shown are the mean ± SD. Statistical analyses were performed with unpaired Student's *t*-tests. **P < 0.01 and ****P < 0.0001.

(c) Histological analysis of ceca from C57BL/6 and *Stat3*$^{fl/fl}$*Ncr1*-iCre mice 9 days after infection. Quantification of cecum crypt length from C57BL/6 and *Stat3*$^{fl/fl}$*Ncr1*-iCre mice (*n* = 8 mice per genotype in total) pooled from two independent experiments. The data shown are means ± SEM. Statistical analyses were performed with unpaired Student's *t*-tests, ***P < 0.001.

(d-e) Characterization of NCR^{+}RORγt^{-} cells and ILC3 populations in different compartments of the gastrointestinal tract. (**d**) Representative flow cytometry plots showing RORγt-GFP and surface NKp46 expression in Lin^{-}CD45^{+} cells isolated from the lamina propria of the small intestine, cecum and colon of naive *Rorc*$^{GFP/+}$ mice. Data is representative of two independent experiments (n=3 per group per experiment) (**e**) WT mice were infected with 10^{10} c.f.u. *C. rodentium* on day 0. Graphs show the ratio of the frequency of the indicated populations on day 8 post-infection (black bars) over that of day 0 (white bars). Representative data from one of two independent experiments are shown (n=6 mice) as means ± SD.

Table 1

Number of differentially expressed genes in ILC3 subsets

Up		NCR⁻ ILC3		NCR⁺ ILC3	
Down		CD4⁺	DN	RORγt^{hi}	RORγt^{int}
NCR⁻ ILC3	CD4⁺		19	1011	744
	DN	20		972	646
NCR⁺ ILC3	RORγt^{hi}	826	751		79
	RORγt^{int}	560	536	84	

Number of differentially expressed genes between each of the ILC3 populations sorted from *Rorc*$^{gfp/+}$ *Tbx21*$^{+/+}$ mice. Rows show genes going up and columns show genes going down in the indicated populations.